Inorganic Chemistry

Article

pubs.acs.org/IC

Redox Levels of a *closo*-Osmaborane: A Density Functional Theory, Electron Paramagnetic Resonance and Electrochemical Study

Alexandr N. Simonov,[†] John F. Boas,[‡] Melissa A. Skidmore,[§] Craig M. Forsyth,[†] Elena Mashkina,[†] Mark Bown,*[,§] and Alan M. Bond*[,†]

[†]School of Chemistry and [‡]School of Physics, Monash University, Clayton, Victoria 3800, Australia

[§]CSIRO Materials Science & Engineering, Bag 10, Clayton South MDC, Victoria 3169, Australia

Supporting Information

ABSTRACT: A *closo*-type 11-vertex osmaborane [1-(η^6-pcym)-1-$OsB_{10}H_{10}$] (pcym = *para*-cymene) has been synthesized and characterized by single-crystal X-ray diffraction and elemental analysis, as well as by ^{11}B and ^{1}H NMR, UV−visible, and mass spectrometry. The redox chemistry has been probed by dc and Fourier transformed ac voltammetry and bulk reductive electrolysis in CH_3CN (0.10 M (n-Bu)$_4NPF_6$) and by voltammetry in the ionic liquid *N*-butyl-*N*-methylpyrrolidinium bis(trifluoromethylsulfonyl)amide ($Pyrr_{1,4}$-NTf_2), which allows the oxidative chemistry of the osmaborane to be studied. A single-crystal X-ray diffraction analysis has shown that [1-(η^6-pcym)-1-$OsB_{10}H_{10}$] is isostructural with other metallaborane compounds of this type. In CH_3CN (0.10 M (n-Bu)$_4NPF_6$), [1-(η^6-pcym)-1-$OsB_{10}H_{10}$] undergoes two well-resolved one-electron reduction processes with reversible potentials separated by ca. 0.63−0.64 V. Analysis based on a comparison of experimental and simulated ac voltammetric data shows that the heterogeneous electron transfer rate constant (k^0) for the first reduction process is larger than that for the second step at GC, Pt, and Au electrodes. k^0 values for both processes are also larger at GC than metal electrodes and depend on the electrode pretreatment, implying that reductions involve specific interaction with the electrode surface. EPR spectra derived from the product formed by one-electron reduction of [1-(η^6-pcym)-1-$OsB_{10}H_{10}$] in CH_3CN (0.10 M (n-Bu)$_4NPF_6$) and electron orbital data derived from the DFT calculations are used to establish that the formal oxidation state of the metal center of the original unreduced compound is Os^{II}. On this basis it is concluded that the metal atom in [1-(η^6-pcym)-1-$OsB_{10}H_{10}$] and related metallaboranes makes a 3-orbital 2-electron contribution to the borane cluster. Oxidation of [1-(η^6-pcym)-1-$OsB_{10}H_{10}$] coupled to fast chemical transformation was observed at 1.6 V vs ferrocene$^{0/+}$ in $Pyrr_{1,4}$-NTf_2. A reaction scheme for the oxidation involving formation of [1-(η^6-pcym)-1-$OsB_{10}H_{10}$]$^+$, which rearranges to an unknown electroactive derivative, is proposed, and simulations of the voltammograms are provided.

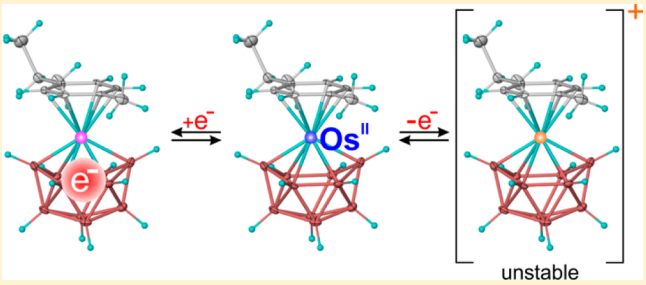

INTRODUCTION

The existence of *closo*-type metallaborane clusters which deviate from the classical Williams−Wade structures[1] has been known for many years.[2,3] Structurally characterized examples are known for 9-, 10- and 11-vertex clusters, and characteristically have the metal atom in a high symmetry, high connectivity position. These alternative *closo* geometry clusters, depending upon how the metal atom is regarded as contributing to the cluster electron count,[2,3] have attracted significant interest because of the structure−bonding implications. If the metal atom is simply regarded as replacing a {B−H} unit in a $[B_nH_n]^{2-}$ structure with a 3-orbital 2-electron (3o−2e) contribution, then a cluster electron count of n electron pairs is achieved. If, however, the metal atom is regarded as making a 4-orbital 4-electron (4o−4e) contribution to cluster bonding, then n + 1 electron pairs are achieved. The *closo*-metallaborane clusters with a 3o−2e contribution from the metal atom (n electron pairs) are often referred to as *hypercloso*[3] to reflect both electron count and geometry, while metallaboranes with *isocloso* geometry (Scheme 1) were initially suggested to have a 4o−4e contribution from the metal center (n + 1 electron pairs).[2,4]

To avoid possible ambiguity,[5] we use a classical nomenclature 3o−2e or 4o−4e to reflect the contribution from the metal center to the cluster,[6] and the term *isocloso* to reflect the geometry but not the number of electron pairs. While the geometries (Scheme 1) of the 9- (**1**) and 10-vertex (**2**) *isocloso* structures differ radically from those of the notional parent clusters [*closo*-B_9H_9]$^{2-}$ (**4**) and [*closo*-$B_{10}H_{10}$]$^{2-}$ (**5**), respectively, the geometry of the *isocloso* 11-vertex cluster is only subtly different from that of the parent 11-vertex cluster [*closo*-$B_{11}H_{11}$]$^{2-}$ (**6**).[7]

Although there are numerous structurally characterized examples of compounds of this type and a substantial number of theoretical papers,[8−14] virtually no experimental data

Received: December 19, 2014
Published: April 21, 2015

DOI: 10.1021/ic503027g
Inorg. Chem. 2015, 54, 4292−4302

Scheme 1. *isocloso*-Metallaborane (1−3) and Parent Borane (4−6) Clusters

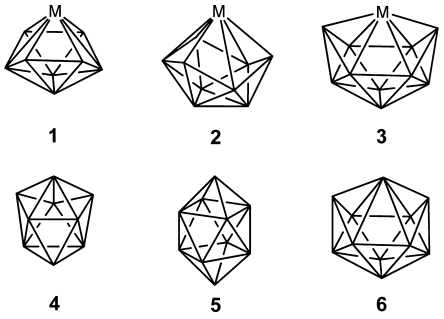

exploring implications in the redox chemistry are available. In principle, the difference in the contribution of the metal center to cluster bonding between 3o−2e and 4o−4e should lead to a difference of 2 in the formal oxidation state so that chemical and electrochemical interconversion should be possible. Although electrochemical studies[15,16] of the 10- and 11-vertex *closo* compounds $[(\eta^6\text{-}C_6Me_6)\text{-}isocloso\text{-}RuB_9H_9]$[17,18] and $[(\eta^6\text{-}C_6Me_6)\text{-}isocloso\text{-}RuB_{10}H_{10}]$[17,19] have been reported and should reflect a difference in oxidation state, the authors do not comment on this feature, nor consider the contribution of the cluster electron count to the electrochemistry. However, Spencer et al.[20] have reported on the reversible interconversion of *hypercloso*-$[1\text{-}(\eta^6\text{-}C_6Me_6)\text{-}1\text{-}RuB_9H_9]$ (structure **2**) and *closo*-$[2\text{-}(\eta^6\text{-}C_6Me_6)\text{-}2\text{-}RuB_9H_9]$ (structure **7**) (Scheme 2) by means of a two-electron chemical reduction using sodium dihydronaphthylide.

Scheme 2. Interconversion between *hypercloso*-$[1\text{-}(\eta^6\text{-}C_6Me_6)\text{-}1\text{-}RuB_9H_9]$ (2) and *closo*-$[2\text{-}(\eta^6\text{-}C_6Me_6)\text{-}2\text{-}RuB_9H_9]$ (7) as Reported in Ref 20

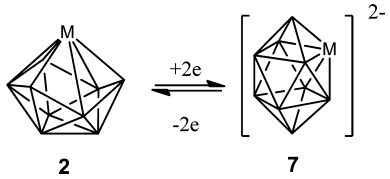

Interestingly, a one-electron oxidation of the dianion (Scheme 2) yields a relatively stable radical anion, *closo*-$[1\text{-}(\eta^6\text{-}C_6Me_6)\text{-}1\text{-}RuB_9H_9]^{\bullet-}$, the ^{11}B nuclear magnetic resonance (NMR) spectrum of which suggests it to have the *hypercloso* structure **2**. The electron paramagnetic resonance (EPR) spectrum of this intermediate consisted of a broad unresolved signal from which no information regarding the structure or the oxidation state of the ruthenium metal center can be gleaned.[20]

Here we describe the synthesis and single-crystal X-ray structure of a new *closo*-type 11-vertex osmium-containing metallaborarane $[1\text{-}(\eta^6\text{-pcym})\text{-}1\text{-}OsB_{10}H_{10}]$ (**8** or $[Os(\eta^6\text{-pcym})(B_{10}H_{10})]$) (pcym = *para*-cymene) along with its dc and Fourier transformed ac voltammetric (FTACV) characterization in the molecular solvent acetonitrile containing 0.10 M $(n\text{-}Bu)_4NPF_6$ as the supporting electrolyte and the room temperature ionic liquid *N*-butyl-*N*-methylpyrrolidinium bis(trifluoromethylsulfonyl)amide ($Pyrr_{1,4}\text{-}NTf_2$). EPR spectroscopic characterization of electrochemically reduced acetonitrile solutions of **8** is used to determine the formal oxidation state of osmium and is combined with the analysis of electron orbital data derived from the density functional theory (DFT) calculations and voltammetry to characterize the redox levels of the *closo*-metallaborane cluster.

EXPERIMENTAL SECTION

Materials. The starting materials $[Os(pcym)Cl_2]_2$[21] and $[NEt_3H]_2[B_{10}H_{10}]$[22] were prepared according to literature methods under an atmosphere of dry nitrogen, although subsequent manipulations were carried out in air.

Tetra(*n*-butyl)ammonium hexafluorophosphate ($(n\text{-}Bu)_4NPF_6$; 98%, Wako), used as the supporting electrolyte in electrochemical experiments, was recrystallized twice from ethanol (96%, Merck Emplura). The ionic liquid $Pyrr_{4,1}\text{-}NTf_2$ (high purity; Merck Millipore) was unpacked inside a nitrogen filled glovebox. CD_2Cl_2 (99.9%; Cambridge Isotope Laboratories Inc.), tetrahydrofuran (≥99.9%, Lichrosolv HPLC grade; Merck), dichloromethane (≥99.8%, BDH), and ferrocene (Fc; 98%, Ega-Chemie) were used as received. Acetonitrile (≥99.9%, Lichrosolv HPLC grade; Merck) used in electrochemical experiments in a glovebox was distilled over CaH_2 under a high-purity N_2 (99.999%, H_2O < 3 ppm, O_2 < 2 ppm) atmosphere. The same N_2 was used to remove oxygen from solutions in electrochemical experiments undertaken on the bench. High-purity water was obtained from an Arium 61315 (Sartorius) water purification system.

Synthesis of $[1\text{-}(\eta^6\text{-pcym})\text{-}1\text{-}OsB_{10}H_{10}]$. $[1\text{-}(\eta^6\text{-pcym})\text{-}1\text{-}OsB_{10}H_{10}]$ was prepared analogously to the procedure documented for the synthesis of a hexamethylbenzeneruthenaborane analogue.[23] A mixture of $[Os(\eta^6\text{-pcym})Cl_2]_2$ (300 mg, 0.38 mmol) and $[NEt_3H]_2[B_{10}H_{10}]$ (245 mg, 0.76 mmol) was stirred for 19 h in dichloromethane. The resulting red solution was filtered over silica gel using dichloromethane. The mother liquor was evaporated to dryness under reduced pressure. ^{11}B NMR spectra of the resulting product dissolved in CD_2Cl_2 showed the presence of a small amount (<5 mol %) of byproduct (most likely $[2\text{-}Cl\text{-}1\text{-}(\eta^6\text{-pcym})\text{-}1\text{-}OsB_{10}H_{10}]$), which was removed by preparative scale high-performance liquid chromatography (HPLC) as described below. The solvent was removed under reduced pressure to give $[1\text{-}(\eta^6\text{-pcym})\text{-}1\text{-}OsB_{10}H_{10}]$ (**8**) (194 mg, 0.44 mmol, 58% yield) as red microcrystals. X-ray quality crystals were grown by vapor diffusion of ether into a saturated dichloromethane solution.

Selected data for **8**: MS (EI) M^+ (max) *m*/*z* 446 (isotopic pattern as calculated for 1 Os and 10 B atoms). Elemental analysis results (calculated): C, 26.82 (27.14); H, 5.46 (5.47).

HPLC. Preparative scale HPLC was performed on the ca. 200 mg scale achieved by dissolving in a minimum (~20 mL) of 20 vol % tetrahydrofuran/20 vol % H_2O/CH_3CN and using a Waters Prep LC 4000 System with a 300 × 40 mm Deltaprep C18 column and a 40 × 40 mm precolumn. UV detection at 292 nm was achieved with a Waters 490E programmable multiwavelength detector. The mobile phase was 60 vol % CH_3CN/H_2O at 80 mL min^{-1}, which gave a retention time for **8** of 18−19 min.

Spectroscopic Characterization of $[1\text{-}(\eta^6\text{-pcym})\text{-}1\text{-}OsB_{10}H_{10}]$. ^1H and ^{11}B NMR spectra were recorded in CD_2Cl_2 using a Bruker AV400 spectrometer. Chemical shifts (δ) are reported in ppm relative Ξ = 100 MHz for $\delta(^1H)$ (nominally TMS), Ξ = 32.094 433 MHz for $\delta(^{11}B)$ (nominally $[BF_3(OEt_2)]$ in $CDCl_3$). Ξ is as defined by McFarlane.[24]

Positive ion EI mass spectra (MS) were obtained with a ThermoQuest MAT95XL mass spectrometer using an ionization energy of 70 eV.

X-ray Structure Determination for $[1\text{-}(\eta^6\text{-pcym})\text{-}1\text{-}OsB_{10}H_{10}]$. A red thin square plate crystal having approximate dimensions of 0.25 × 0.25 × 0.05 mm was covered in viscous oil and mounted on a Bruker ApexII CCD diffractometer. X-ray data were collected at 123 K using graphite monochromated Mo Kα radiation (λ = 0.071073 Å) to $2\theta_{max}$ = 55.0°. The Bruker Apex2 v2012-2.0 software package[25] was used for data processing, which included a multiscan absorption correction (SADABS 2008-1).[26] The structure was solved using the metal atom coordinates for the known Ru analogue,[23] and refined with full matrix least-squares on F^2, using SHELXL97.[27] All non-hydrogen

DOI: 10.1021/ic503027g
Inorg. Chem. 2015, 54, 4292−4302

atoms were refined with anisotropic thermal parameter forms. Hydrogen atoms attached to C were placed in calculated positions with C−H 0.95−1.00 Å and $U_{iso}(H) = 1.2/1.5 \times U_{eq}(C)$. For consistency with the analogous Ru structure,[23] hydrogen atoms associated with B were located and refined with B−H distances restrained to be similar within 0.02 Å. The final weighting scheme was $w = 1/[\sigma^2(Fo^2) + (aP)^2 + bP]$ where $P = (F_o^2 + 2F_c^2)/3$ ($a = 0.0097$, $b = 7.1951$).

The crystallographic data and the refinement parameters of [1-(η^6-pcym)-1-$OsB_{10}H_{10}$] are as follows: FW 442.59; orthorhombic *Pbca*; $a = 7.7693(3)$, $b = 14.0374(5)$, $c = 29.9826(12)$ Å; volume = 3269.9(2) Å^3; $\rho_{calc} = 1.798$ g cm^{-3} ($Z = 8$); $\mu = 7.779$ mm^{-1}; $N_{total} = 13734$, $N = 3731$; R1 = 0.022, wR2 = 0.048 (for 3385 reflections with $I > 2\sigma(I)$), R1 = 0.025, wR2 = 0.050 (all data); GoF = 1.095; $\Delta\rho$(max, min) = 0.93, −1.27 e Å^{-3}.

Electrochemical Instrumentation and Procedures. Electrochemical experiments were undertaken in a three-electrode configuration at ambient temperature (297 ± 1 K) using either an Epsilon electrochemical workstation (BAS) or a custom-made FTACV instrument.[28] For voltammetric studies in acetonitrile (0.10 M (n-Bu)$_4$NPF$_6$), deoxygenation was provided by purging with solvent saturated nitrogen for 15−20 min. Voltammetric measurements in $Pyrr_{1,4}$-NTf_2 ionic liquid and controlled potential bulk electrolysis experiments in CH_3CN (0.10 M (n-Bu)$_4$N-PF$_6$) were undertaken inside a nitrogen filled glovebox. Prior to each experiment, all glassware was filled with acetone (≥99.0%, Merck Emplura) and sonicated for at least 10 min, washed repeatedly with fresh portions of acetone, and dried in a N_2 stream and then in an oven at ca. 130 °C for at least 30 min.

In voltammetric studies, glassy carbon (GC, nominal diameter 1 or 3 mm), gold (nominal diameter 1 mm), platinum (nominal diameter 2 mm), or boron-doped diamond (BDD, nominal diameter 3 mm) macrodisk electrodes embedded in an isolating inert sheath (BAS) or a carbon fiber microelectrode (nominal diameter 11 μm) were employed as the working electrodes. Prior to commencing an experiment, the surface of the working electrode was thoroughly polished with alumina powder (Buehler; 0.3 and 0.05 μm for macrodisk electrodes and microelectrode, respectively) on a wet polishing cloth (BAS). After polishing, the electrode was washed repeatedly with water and subjected to sonication (FXP 10M, U-LAB Instruments) in water for ca. 20 s. To ensure complete removal of the alumina powder from the electrode surface after sonication, the electrode was carefully wiped for at least 50 times with a clean wet Al_2O_3-free polishing cloth, washed with water, and again sonicated for ca. 20 s in a fresh portion of H_2O. Finally, the working electrode surface was flushed with acetone and dried in a nitrogen stream. The electroactive surface areas of the macrodisk electrodes and the diameter of the microelectrode were estimated respectively[29] from the Randles−Ševčik relationship that applies in transient linear sweep voltammetry and the diffusion limited current value obtained under near steady-state voltammetric conditions, using oxidation of ferrocene in acetonitrile (0.10 M (n-Bu)$_4$NPF$_6$) and assuming the value for the diffusion coefficient (D) of Fc^0 is 2.4×10^{-5} cm^2 s^{-1} in this medium.[30] Unless otherwise stated, current data are normalized to the electrode surface area.

High surface area Pt wire in contact with solvent (electrolyte) and separated from the working electrode compartment by a glass frit and Pt wire installed inside a Luggin capillary positioned in the vicinity of the surface of the working electrode were used as auxiliary and quasi-reference electrodes, respectively. The potential of the quasi-reference electrode was calibrated vs the reversible potential of the $Fc^{0/+}$ couple measured in the same solution as the voltammetric experiment on the osmaborane compound.

For exhaustive reductive electrolysis of [Os(η^6-pcym)($B_{10}H_{10}$)] in CH_3CN (0.10 M (n-Bu)$_4$NPF$_6$), Pt gauze was used as the working and auxiliary electrodes, and Pt wire was used as a quasi-reference electrode. Auxiliary and quasi-reference electrode compartments containing solvent (electrolyte) were separated from the working electrode chamber with fine porosity glass frits. During electrolysis, the solution in the working electrode compartment was vigorously agitated by a magnetic stirrer.

Spectroscopic Studies. UV−vis spectra of [Os(η^6-pcym)-($B_{10}H_{10}$)] in CH_3CN (0.10 M (n-Bu)$_4$NPF$_6$) and the products formed after reductive electrolysis were recorded with a Varian Cary 5000 spectrophotometer in a 10 mm quartz cuvette.

EPR spectra were obtained with a Bruker ESP380E CW/FT X-band (ca. 9.4 GHz) spectrometer using a standard TE_{102} rectangular cavity. A nitrogen gas flow insert and a Bruker VT4111 temperature controller were used for experiments at 120 K, and a finger dewar inserted into the cavity was used to obtain a sample temperature of 77 K. Microwave frequencies were measured with an EIP microwave 548A frequency counter, and g values were determined with reference to the F^+ resonance in CaO with $g = 2.0001 \pm 0.0001$.[31] Spectra were recorded as the first derivative of the absorption and were simulated with the XSophe-Sophe-XeprView software.[32] Uncertainties in the g values obtained at X-band frequencies were estimated as being ±0.002.

Theory. Simulations of dc and ac voltammograms were undertaken using DigiElch-Professional 7.F[33] and Monash Electrochemistry Simulator (MECSim)[34] software packages, respectively. Electrode kinetic parameters were recovered from comparisons of experimental FT ac voltammetric data with simulations on the basis of the "best fit" criteria (viz., lowest objective function defined by eq 1) aided by e-science methods available in the Nimrod/O tool kit.[35]

$$\Psi_{nim}(H) = \frac{1}{H}\cdot\sum_{h=1}^{H}\sqrt{\frac{\sum_{i=1}^{N}(f_h^{exp}(x_i) - f_h^{sim}(x_i))^2}{\sum_{i=1}^{N}f_h^{exp}(x_i)^2}}, \quad (1)$$

where h is the number of the ac harmonic component, H is the total number of the components evaluated, $f_h^{exp}(x)$ and $f_h^{sim}(x)$ are the experimental and simulated functions in the corresponding component, respectively, and N is the number of data points.

To minimize the influence of the ringing artifact associated with inverse Fourier transform procedure,[36] the first and the last 5 s of the voltammetric data set were ignored in automated experiment-simulation comparisons.

Quantum chemistry calculations were carried out using density functional theory (DFT) as implemented in the Gaussian 09 suite of programs.[37] Full geometry optimizations were undertaken using the B3LYP exchange-correlation functional.[38] The geometry of the gas phase target compounds was optimized at the B3LYP spin-restricted level of theory using the LAN2DZ basis set for osmium and 6-31+G(d) basis set for all other atoms. Vibrational frequency calculations were performed to verify that the optimized geometries corresponded to minima on the potential energy surface. Single point energy calculations and population analysis were then conducted employing the optimized geometries using the LAN2DZ basis set for osmium and a larger 6-311+G(d,p) basis set for all other atoms. The structures, total and relative energies, and relevant interatomic distances for all calculated systems are given in the Supporting Information.

RESULTS AND DISCUSSION

Synthesis and Spectroscopic Characterization of [1-(η^6-pcym)-1-$OsB_{10}H_{10}$] (8). Reaction of [Os(η^6-pcym)Cl_2]$_2$ with [NEt_3H]$_2$[$B_{10}H_{10}$] in dichloromethane yields red microcrystals of [1-(η^6-pcym)-1-$OsB_{10}H_{10}$] (**8**) in 58% yield. Compound **8** was characterized by ^{11}B and ^{1}H NMR, mass spectroscopy, elemental analysis, and single-crystal X-ray diffraction. All data are consistent with the formulation [($MeC_6H_4{}^iPr$)$OsB_{10}H_{10}$].

The ^{11}B and ^{1}H NMR data are summarized in Table 1. A comparison of the ^{11}B and ^{1}H NMR shielding patterns with those of other well-characterized *closo*-type 11-vertex metallaboranes[4,39,40] and the analogous ruthenium compound [1-(η^6-pcym)-1-$RuB_{10}H_{10}$][23] shows that **8** has the same electronic and geometric structure. The ^{11}B NMR spectrum consists of four

DOI: 10.1021/ic503027g
Inorg. Chem. 2015, 54, 4292−4302

Table 1. ^{11}B and ^{1}H NMR Data for [1-(η^6-pcym)-1-$OsB_{10}H_{10}$] (8) in CD_2Cl_2

assignment[a]	$\delta(^{11}B)$/ppm [$^{1}J(^{11}B-^{1}H)$/Hz]	$\delta(^{1}H)$/ppm[b,c]
2, 3	(2B) 93.03 [149]	(2H) 12.08
10, 11	(2B) 17.48 [142]	(2H) 2.90
8, 9	(2B) 11.80 [137]	(2H) 5.18
4, 5, 6, 7	(4B) 4.81 [144]	(4H) 0.50

[a]Assignment made on the basis of ^{11}B-{^{1}H} COSY. [b]Assignment made on the basis of ^{1}H−^{11}B HSQC. [c]$\delta(^{1}H)$ ($MeC_6H_4Pr^i$): Me 2.21; C_6H_4 6.50 (d) and 6.41 (d) [$^{3}J(^{1}H-^{1}H)$ = 6.5 Hz]; C*H*Me$_2$ 2.79 (heptet) [$^{3}J(^{1}H-^{1}H)$ = 6.9 Hz]; CH*Me*$_2$ 1.15 (d) [$^{3}J(^{1}H-^{1}H)$ = 6.9 Hz].

resonances in a 2:2:2:4 ratio, each showing coupling to an *exo*-terminal hydrogen atom. The ^{11}B resonances were unambiguously assigned using ^{11}B-{^{1}H} COSY. The ^{1}H NMR spectrum shows the presence of the resonances expected for an osmium bound η^6-pcym ligand,[21] and the ^{1}H-{^{11}B} spectrum reveals the presence of the *exo*-terminal hydrogen atoms associated with the borane cage. These resonances were unambiguously assigned to the boron atoms to which they are attached using ^{1}H−^{11}B HSQC. The ^{11}B and ^{1}H NMR shielding patterns of this type of *closo* 11-vertex cluster are particularly characteristic with two boron atoms having low field ^{11}B resonances at $\delta(^{11}B)$ ca. 90 ppm [B(2,3)] that are associated with two hydrogen atoms having ^{1}H resonances at $\delta(^{1}H)$ ca. 12 ppm, and eight boron atoms [B(4−11)] having ^{11}B resonances at $\delta(^{11}B)$ ca. 10 ppm associated with eight hydrogen atoms a having ^{1}H resonances in the range $\delta(^{1}H)$ 0−5 ppm. These shielding patterns are regarded as being diagnostic of this structural type.[41]

X-ray Crystallographic Analysis of [1-(η^6-pcym)-1-$OsB_{10}H_{10}$] (8). The molecular structure of **8** as determined by single-crystal X-ray analysis is shown in Figure 1, with the atom numbering; selected bond distances and interatomic angles being given in Table 2.

Compound **8** is isostructural with the ruthenium analogue characterized previously.[23] The geometry of the {$OsB_{10}H_{10}$} substructure deviates little from the expected C_{2v} symmetry with the bond lengths between the lower connectivity apical

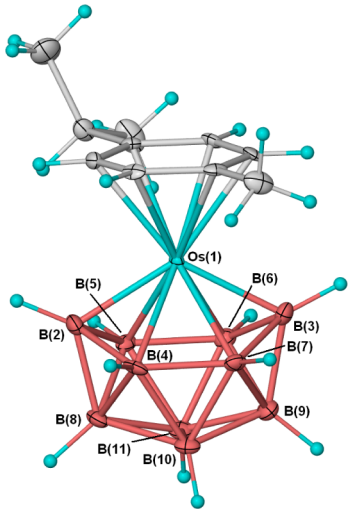

Figure 1. Molecular structure of [1-(η^6-pcym)-1-$OsB_{10}H_{10}$] (**8**) with 50% ellipsoids.

Table 2. Selected Bond Lengths for [1-(η^6-pcym)-1-$OsB_{10}H_{10}$] (8)

bond	length/Å	bond	length/Å
osmium−boron			
Os−B(2)	2.102(4)	Os−B(3)	2.112(4)
Os−B(4)	2.287(3)	Os−B(5)	2.302(4)
Os−B(6)	2.304(4)	Os−B(7)	2.287(4)
osmium−carbon			
Os−C(1)	2.345(3)	Os -C(2)	2.312(3)
Os−C(3)	2.338(3)	Os -C(4)	2.349(3)
Os -C(5)	2.294(3)	Os -C(6)	2.321(3)
boron−boron			
B(2)−B(4)	1.754(6)	B(3)−B(7)	1.767(5)
B(2)−B(5)	1.759(5)	B(3)−B(6)	1.769(6)
B(2)−B(8)	1.711(5)	B(3)−B(9)	1.722(5)
B(4)−B(7)	1.741(5)		
B(4)−B(8)	1.841(5)	B(7)−B(9)	1.838(6)
B(4)−B(10)	1.799(5)	B(7)−B(10)	1.793(5)
B(5)−B(6)	1.735(5)		
B(5)−B(8)	1.848(5)	B(6)−B(9)	1.838(6)
B(5)−B(11)	1.803(5)	B(6)−B(11)	1.797(5)
B(8)−B(10)	1.783(6)	B(9)−B(10)	1.774(6)
B(8)−B(11)	1.782(5)	B(9)−B(11)	1.770(6)
B(10)−B(11)	1.762(5)		

boron atoms [Os−B(2),B(3) = 2.107 Å (average)] being significantly shorter than those to the higher connectivity boron atoms [Os−B(4),B(5),B(6),B(7) = 2.295 Å (average)]. The connectivity and bond lengths of the osmium atom to the {$B_{10}H_{10}$} subcluster and the boron−boron bond lengths within the cluster are typical of this class of 11-vertex *closo*-type metallaborane,[42] and make it a good candidate for investigations into the nature of the electronic bonding within this general class of compound.

DFT Modeling of the Structure and Electronic Properties of [1-(η^6-pcym)-1-$OsB_{10}H_{10}$] (8). In order to gain further understanding of the structural and electronic properties of [Os(η^6-pcym)($B_{10}H_{10}$)], we undertook DFT calculations and compared results with those for the [*closo*-$B_{11}H_{11}^{2-}$] and [*hypercloso*-$B_{11}H_{11}$] clusters (Table S1, Supporting Information). The optimized structures of [*closo*-$B_{11}H_{11}^{2-}$] and [*hypercloso*-$B_{11}H_{11}$] are topologically equivalent (Figure S1, Supporting Information), but some variations in bond lengths are observed. In particular, in [*closo*-$B_{11}H_{11}^{2-}$], the bond distances B1−B3 (= B2−B6, B1−B4, B2−B6, B2−B6) are 1.67 Å, B1−B21 (= B2−B21) 1.78 Å, B1−B7 (= B2−B8) 1.76 Å, and B4−B5 (= B2−B4) 1.87 Å, while the corresponding bond lengths in [*hypercloso*-$B_{11}H_{11}$] are 1.73 Å, 1.74 Å, 1.84 Å, and 1.68 Å (see Figure S1, Supporting Information, for atom labeling), consistent with the literature data.[11] Shortening of the B2−B21 bond and lengthening of the B4−B5 bonds converts the *hypercloso* structure to the *closo* one. The corresponding bond distances in [Os(η^6-pcym)($B_{10}H_{10}$)] are as follows: B1−B3 (= B2−B6, B1−B4, B2−B6, B2−B6) 1.76 Å, B1−Os (= B2−Os) 2.11 Å, B1−B7 (= B2−B8) 1.71 Å, and B4−B5 (= B2−B4) 1.74 Å. The calculated parameters of the compound are in good agreement with the crystal structure determined (Table S2, Supporting Information), but do show the typical slight overestimation of bond lengths found in other studies with respect to the experimental data.[43]

Contours of the HOMO, LUMO, HOMO-1, and LUMO+1 distributions of [Os(η^6-pcym)($B_{10}H_{10}$)] are illustrated in Figure

DOI: 10.1021/ic503027g
Inorg. Chem. 2015, 54, 4292−4302

2. The regional separation of orbital distribution in the HOMO and LUMO is clearly shown; the orbitals of the HOMO are

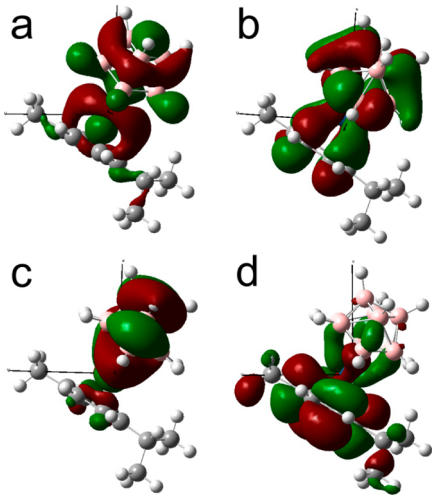

Figure 2. Contours of the (a) HOMO, (b) LUMO, (c) HOMO-1, and (d) LUMO+1 distributions of [Os(η^6-pcym)($B_{10}H_{10}$)].

localized on the central Os atom and $B_{10}H_{10}$ and the LUMO located on the $B_{10}H_{10}$ cluster and *para*-cymene. The donation of the d orbital of osmium is significant, where the calculated electron population of the HOMO is 65%, indicating strong mixing of the d orbitals. The HOMO − 1 shows a mixing of the boron orbitals (12, 11, 17, and 18) with those of osmium; the calculated electron population is ∼15% for each. The calculated electron population of the LUMO is made up of contributions from boron orbitals 11 and 12 to the *para*-cymene C3 and C6.

Visually it can be seen that the electron density lies in the *xy* plane, and analysis of the orbital coefficients for the HOMO (Table S3, Supporting Information) shows that it is composed predominantly of the osmium d_{xy} orbital with smaller contributions from the $d_{x^2+y^2}$ basis functions. The calculated electron population of the one-electron reduced state of the cluster shows that the electron is highly delocalized, with only a small amount of electron density located on the Os center. The bulk of the electronic density of the SOMO is located across the boron cluster, with ca. 6% allocated to the osmium d orbital.

Dc Cyclic Voltammetry of [1-(η^6-pcym)-1-$OsB_{10}H_{10}$] (8) in CH_3CN. Dc cyclic voltammograms of [Os(η^6-pcym)($B_{10}H_{10}$)] in acetonitrile (0.10 M (n-Bu)$_4$NPF$_6$) contain two well-defined chemically reversible reduction processes separated by ca. 0.63−0.64 V (Figure 3). A linear dependence of the

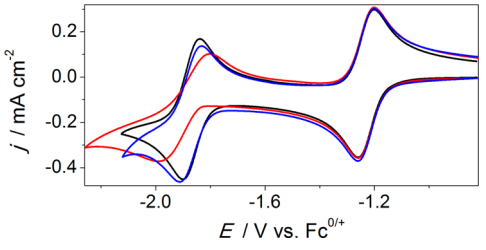

Figure 3. Dc cyclic voltammograms (v = 0.10 V s^{-1}) for reduction of 1.0 mM [Os(η^6-pcym)($B_{10}H_{10}$)] in CH_3CN (0.10 M (n-Bu)$_4$NPF$_6$) with well-polished GC (black) and Pt before (red) and after (blue) cycling the potential to 1.6 V at 297 K.

reduction peak currents (I^p_{red}) on concentration of [Os(η^6-pcym)($B_{10}H_{10}$)] (0.2−1 mM) and the square root of the scan rate (v = 0.04−1.5 V s^{-1}) confirms the diffusion-controlled nature[29] of both these processes.

The peak-to-peak separations of reduction and oxidation peak potentials ($\Delta E^p = E^p_{ox} - E^p_{red}$), which reflect the electrode kinetics of the [Os(η^6-pcym)($B_{10}H_{10}$)] reduction processes, were found to be very sensitive to the nature of pretreatment of the electrode surface. The ratio of the reduction and oxidation peak currents (I^p_{red}/I^p_{ox}) was close to unity, and ΔE^p were ca. 0.065 V, which are expected for a fast one-electron process[29] with uncompensated resistance (R_u) of 40−50 Ω, for the first reduction process with well-polished GC (Figure 3a, black curve), Pt (Figure 3a, blue and red curves), and Au (not shown). Similar I^p_{red}/I^p_{ox} and ΔE^p values expected for a fast one-electron transfer process also were found for the second reduction step with extensively polished GC, but not with Pt and Au electrodes, where ΔE^p values of ≥0.14 V (red curve in Figure 3a) were found even after intensive polishing. Faster kinetics of the [Os(η^6-pcym)($B_{10}H_{10}$)] reduction with metal electrodes is achieved by applying very positive potentials in cyclic voltammograms of up to 1.6 V vs $Fc^{0/+}$ (Figure 3), but even then ΔE^p for the second reduction step of ≥0.080 V are obtained with Pt and Au (Figure 3a).

Midpoint potentials (E_m) for the first and second [Os(η^6-pcym)($B_{10}H_{10}$)] reduction processes in CH_3CN (0.10 M (n-Bu)$_4$NPF$_6$) calculated as ($E^p_{ox} + E^p_{red}$)/2 with well-polished electrodes were −1.230 ± 0.003 and −1.865 ± 0.003 V, respectively. Qualitatively similar dc cyclic voltammetric behavior was reported for reduction of [1-(η^6-C_6Me_6)-*closo*-1-$RuB_{10}H_{10}$] in dichloromethane with a GC electrode.[16] No processes that could be unambiguously attributed to oxidation of [Os(η^6-pcym)($B_{10}H_{10}$)] could be detected within the available potential window under these conditions (Figure S2, Supporting Information).

The redox chemistry of metallacarborane and metallaborane clusters can be arbitrarily assigned to changes in the formal oxidation state of a metal,[44−46] although the metal atom represents an integral part of a cluster acting as a "surrogate" boron atom.[42,47] Nevertheless, an assignment of the changes in the apparent oxidation state of the Os atom can be probed voltammetrically. It is well-known that the ligand environment influences the reversible potentials (E^0) of $Me^{n/m}$ processes,[45,46,48] and hence the E^0 values obtained for [Os(η^6-pcym)($B_{10}H_{10}$)] are of limited use in establishing the formal oxidation state of osmium within the metallaborane cluster. Spectroscopic data are needed for this purpose.

Reductive Bulk Electrolysis of [1-(η^6-pcym)-1-$OsB_{10}H_{10}$] (8) in CH_3CN and Spectroscopic Characterization of the Reduction Products. The chemical reversibility of the [Os(η^6-pcym)($B_{10}H_{10}$)] reduction processes suggests that sufficient stability of the reduced forms may allow their spectroscopic characterization. The one-electron stoichiometry for each reduction process assigned on the basis of dc cyclic voltammetry (Figure 3a) was confirmed by coulometric analysis of data derived from exhaustive bulk electrolysis of [Os(η^6-pcym)($B_{10}H_{10}$)] at controlled potentials of −1.34 and −2.04 V. Both the one- and two-electron reduced species produced by bulk electrolysis in CH_3CN were stable for at least several hours under a high-purity nitrogen atmosphere, thereby enabling their voltammetric (Figure S3, Supporting Information), UV−vis (Figure 4), and EPR (Figure 5) characterization.

DOI: 10.1021/ic503027g
Inorg. Chem. 2015, 54, 4292−4302

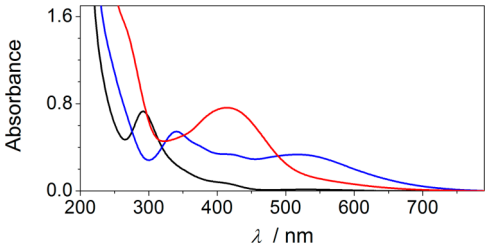

Figure 4. UV−vis spectra of 0.20 mM [Os(η^6-pcym)($B_{10}H_{10}$)] in CH_3CN (0.10 M (n-Bu)$_4NPF_6$) under N_2 atmosphere before (black) and after exhaustive bulk electrolysis at controlled potentials of −1.34 (blue) and −2.04 V (red). Optical path length 10 mm.

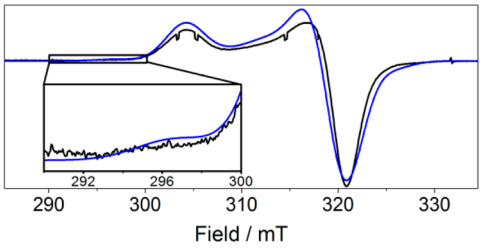

Figure 5. EPR spectrum at 77 K derived from the one-electron reduction of 0.20 mM [Os(η^6-pcym)($B_{10}H_{10}$)] in CH_3CN (0.10 M (n-Bu)$_4NPF_6$) (black) and simulated EPR spectrum (blue) (see text for the simulation parameters). Inset shows an expanded plot in the outlined range. Spectrometer settings: microwave frequency 9.309 GHz; microwave power 4.18 mW; receiver gain 1.0 × 10^4; 100 kHz modulation amplitude 0.2 mT; field scan range/time 50 mT/84 s; time constant 82 ms.

The UV−vis spectrum of the rose-tinted 0.20 mM [Os(η^6-pcym)($B_{10}H_{10}$)] solution in CH_3CN (0.10 M (n-Bu)$_4NPF_6$) exhibits a major absorption band with maximum absorbance at λ_{max} = 292 nm and shoulder with a λ_{max} value of ca. 416 nm (Figure 4; black curve). One-electron reduction of the osmaborane solution produces a purple colored solution and major changes in the UV−vis spectra. In particular, the main absorption band is now at λ_{max} = 341 nm and accompanied by a broad peak with λ_{max} ≈ 518 nm (Figure 4; blue curve). Further reduction at −2.04 V generates a rich yellow solution with a UV−vis spectrum exhibiting a broad absorption band with λ_{max} = 414 nm, presumably resulting from superposition of several absorption bands (Figure 4). Although the interpretation of the frontier orbital analysis should be treated with caution, the computational results (Table S4 and Figure S4, Supporting Information) suggest a bathochromic shift from [Os(η^6-pcym)($B_{10}H_{10}$)]^0 to the reduction products, consistent with the observed UV−vis spectra.

Prior to reductive electrolysis, no EPR resonance was observed at 120 K from 0.2 mM frozen solutions of [Os(η^6-pcym)($B_{10}H_{10}$)] in CH_3CN (0.1 M (n-Bu)$_4NPF_6$). The EPR spectrum of a frozen sample at 77 K derived from exhaustive controlled potential reduction electrolysis in solution at −1.34 V at 297 K is shown in Figure 5. A solution frozen to 120 K after exhaustive one-electron electrolysis gave an essentially identical spectrum. The same EPR spectrum, but with an intensity at least a factor of 10 times lower, was observed after reductive electrolysis at −2.04 V. The spectrum shown in Figure 5 exhibits axial symmetry and was simulated with $g_{\|}$ = 2.187, $g_{\perp}$ = 2.080 using a Gaussian line shape width of 23 × 10^{-4} cm^{-1}. Weak and poorly resolved features were observed at high spectrometer gains at magnetic fields of around 295, 312, and 328 mT. These are interpreted as being due to hyperfine interactions of the unpaired electron with the 16.1% abundant ^{189}Os nucleus with a nuclear spin I = 3/2. Spectrum simulations lead to hyperfine interaction parameters of $A_{\|}$ = 60 × 10^{-4} cm^{-1} and $A_{\perp}$ = 45 × 10^{-4} cm^{-1}. Hyperfine resonances due to the 1.6% abundant ^{187}Os (I = 1/2) are expected to be of too low an intensity to be observed.[49]

If we consider the present g values as being due to one of the possible formal oxidation states of paramagnetic Os ions, we can exclude Os^{III} on the grounds that the g values are not consistent with those of other ions with the low-spin d^5 electron configuration for which at least one g value is always less than the free electron value of 2.0023.[50−52] The formal oxidation state Os^{-I} is excluded on electrochemical grounds. Interpretation of the g values in terms of a formal oxidation state Os^{I} implies that the paramagnetic electron is located in the in-plane orbitals with d_{xy} and/or $d_{x^2+y^2}$ character rather than in the more common d_{z^2} orbital usually found for the d^7 ions. This would imply that the Os^{I} ion is in a compressed tetragonal environment as distinct from the most common and energetically favored elongated tetragonal environment. Although EPR spectra appearing to be due to d^7 ions in a compressed tetragonal environment are not unknown, they are generally found to be artifactual and to occur as a consequence of Jahn−Teller effects.[53] The present spectra show no evidence for the presence of such effects.

The placement of the unpaired electron in the d_{xy} and/or $d_{x^2+y^2}$ orbitals would, at first sight, appear to be consistent with the results of the DFT calculations. However, the small $\Delta g = g_{\|} - g_{\perp}$ = 0.107, the small $\Delta A = A_{\|} - A_{\perp}$ = 15 × 10^{-4} cm^{-1}, the low magnitude of the hyperfine interactions when compared to those of Os^{I} in, e.g., electron-irradiated $K_4Os(CN)_6$,[54] and an estimate of the d-electron spin density on the Os ion of 30% made using simple crystal field theory[55] all indicate that the unpaired electron is highly delocalized. In this context, it needs to be recognized that the metallaboranes are more satisfactorily regarded as compounds where the unpaired electron is highly delocalized into a set of cluster orbitals and where the bonding involves a significant contribution from the ligand orbitals rather than being predominantly metal-centered.[6] The overlap with the Os d orbitals is sufficient to shift the g values from the free electron value and contribute to the hyperfine interaction. The Os hyperfine interaction in the present case, when averaged on the assumption that the signs of the components are the same, is 50 × 10^{-4} cm^{-1} or approximately 150 MHz, which may be compared with the value of 155 MHz found by Takaoka et al.[56] for the metalloradical [SiP^{iPr}_3]Os($NC_6H_4CF_3$). In the latter case, the suggestion is that some 39% of the spin density is located at the metal center, and that the complex is best considered as an Os^{II} complex with a ligand-localized radical. Although such spin density calculations and comparisons with estimates from DFT calculations can only be considered as crude approximations, the estimate of approximately 30% spin density at the Os metal center as estimated above reinforces the argument that the present one-electron-reduced Os metallaborane complex is best regarded as an Os^{II} complex with a ligand-localized radical.

Electrode Kinetics for Reduction of [1-(η^6-pcym)-1-$OsB_{10}H_{10}$] (8) in CH_3CN. ΔE^p values of about 0.065 V with R_u = 40−50 Ω derived from dc cyclic voltammograms for reduction of [Os(η^6-pcym)($B_{10}H_{10}$)] in CH_3CN (0.10 M (n-Bu)$_4NPF_6$) under conditions of Figure 3 imply that the reaction approaches closely to the "reversible" limit on the

DOI: 10.1021/ic503027g
Inorg. Chem. 2015, 54, 4292−4302

relevant dc voltammetric time scale. Consequently, quantification of the electrode kinetics associated with the $[Os(\eta^6\text{-pcym})(B_{10}H_{10})]^{0/-/2-}$ processes requires the use of a more kinetically sensitive technique, like Fourier transformed (FT) ac voltammetry.[28] Examination of the harmonic components of the FT ac voltammograms obtained for both $[Os(\eta^6\text{-pcym})(B_{10}H_{10})]$ reduction processes in acetonitrile with GC and Pt electrodes (Figures 6 and S3, Supporting Information) shows

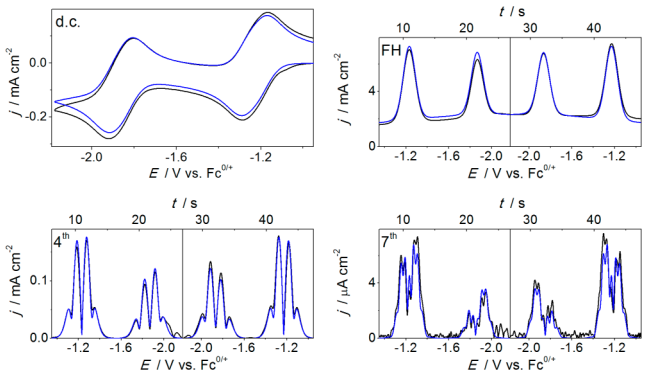

Figure 6. Aperiodic dc and ac fundamental, 4th harmonic, and 7th harmonic components of FT ac voltammograms (v = 0.05961 V s^{-1}; f = 219 Hz; ΔE = 0.080 V) for reduction of 1.0 mM $[Os(\eta^6\text{-pcym})(B_{10}H_{10})]$ in CH_3CN (0.10 M $(n\text{-Bu})_4NPF_6$) with a GC electrode (black) and simulated data (blue). Simulation parameters: R_u = 45 Ω; nonlinear potential dependent double-layer capacitance, $C_{dl}(E)$, model; $E^0_{0/-}$ = −1.228 V, $E^0_{-/2-}$ = −1.862 V; $k^0_{0/-}$ = 1.7 cm s^{-1}, $k^0_{-/2-}$ = 0.22. cm s^{-1}; $\alpha_{0/-}$ = 0.73, $\alpha_{-/2-}$ = 0.62.

well-defined faradaic signals with current magnitudes that are essentially independent of the dc potential sweep direction. These observations are consistent with fast electrode kinetics and chemically reversible electron transfer. The relatively smaller harmonic components for the second process imply that the electron transfer kinetics for the $[Os(\eta^6\text{-pcym})(B_{10}H_{10})]^{-/2-}$ process is slower than for the $[Os(\eta^6\text{-pcym})(B_{10}H_{10})]^{0/-}$ one. This effect is more pronounced with Pt electrodes as deduced from analysis of the dc voltammetric data (Figure 3).

The reversible potentials (E^0) and electrode kinetic parameters (k^0 and α) for the $[Os(\eta^6\text{-pcym})(B_{10}H_{10})]^{0/-/2-}$ processes were estimated via data optimization procedures implemented with Nimrod/O software. In this procedure, comparisons of the experimental FT ac voltammetric data were made with simulations based on a planar diffusion and Butler−Volmer charge transfer kinetics for each of the one-electron processes:

$$[Os(\eta^6\text{-pcym})(B_{10}H_{10})]^0 + e^- \rightleftarrows [Os(\eta^6\text{-pcym})(B_{10}H_{10})]^- \quad (2)$$

$$[Os(\eta^6\text{-pcym})(B_{10}H_{10})]^- + e^- \rightleftarrows [Os(\eta^6\text{-pcym})(B_{10}H_{10})]^{2-} \quad (3)$$

The value of R_u used in simulations was derived from analysis of electrochemical impedance spectra obtained at potentials devoid of faradaic current and use of a simple RC circuit. Potential-dependent double-layer capacitance model $C_{dl}(E)$ was determined for each data set as described elsewhere.[35]

E^0, k^0, and α for the $[Os(\eta^6\text{-pcym})(B_{10}H_{10})]^{0/-}$ process ($E^0_{0/-}$, $k^0_{0/-}$, and $\alpha_{0/-}$, respectively) were derived from the analysis of ac voltammograms (f = 219 Hz) obtained in the potential range pertaining to the first reduction step. These parameters were subsequently used in simulations for recovery of $E^0_{-/2-}$, $k^0_{-/2-}$, and $\alpha_{-/2-}$ for the $[Os(\eta^6\text{-pcym})(B_{10}H_{10})]^{-/2-}$ process from the Nimrod/O-assisted analysis of ac voltammograms (f = 219 and 9 Hz for GC and Pt, respectively) obtained over a potential range that covered both reduction steps.

The diffusion coefficients of $[Os(\eta^6\text{-pcym})(B_{10}H_{10})]^0$, $[Os(\eta^6\text{-pcym})(B_{10}H_{10})]^-$, and $[Os(\eta^6\text{-pcym})(B_{10}H_{10})]^{2-}$ in CH_3CN (0.10 M $(n\text{-Bu})_4NPF_6$) used in simulations were estimated as 1.4 × 10^{-5}, 1.3 × 10^{-5}, and 1.0 × 10^{-5} cm^2 s^{-1}, respectively, from the microelectrode diffusion limited currents (Figure S3, Supporting Information) measured versus reference data derived from oxidation of a known concentration of Fc with D_{Fc} = 2.4 × 10^{-5} cm^2 s^{-1}.[30]

The strategy defined above provided a good level of experiment−theory agreement (Figures 6 and S2, Supporting Information) and reproducible recovery of consistent sets of parameters (Table 3) when using well-polished electrodes. In confirmation of qualitative considerations derived from dc cyclic voltammograms, $k^0_{0/-}$ was substantially higher than $k^0_{-/2-}$ at both Pt and GC electrodes, and the kinetics of electron transfer at Pt is much slower than at GC. This rate order is not consistent with arguments based on the density of states (DOS) theory commonly employed to explain the electrode dependence of k^0 for the outer sphere charge transfer process,[57] since the DOS of GC is lower than that of Pt.[58] Arguably, the processes are inner sphere and hence show electrode dependence based on a specific interaction of the osmaborane cluster with the electrode surface.

At the lower frequency (9 Hz), the experimental ac voltammetric data are satisfactorily mimicked by simulations based on two consecutive one-electron transfer processes with kinetics obeying Butler−Volmer formalism with α = 0.50 (Figure S5, Supporting Information). In contrast, best fit of the experimental ac voltammetric data at higher f = 219 Hz is

Table 3. E^0, k^0, α, and Objectives (Ψ) Recovered by Nimrod/O[a] by Fitting the Models Based on Reactions 2 and 3 under Conditions of FT Ac Voltammograms (f = 219 and 9 Hz) to Experimental Data for Reduction of $[Os(\eta^6\text{-pcym})(B_{10}H_{10})]$ in CH_3CN (0.10 M $(n\text{-Bu})_4NPF_6$) at Pt and GC Electrodes[b]

	E^0/V vs $Fc^{0/+}$		k^0/cm s^{-1}		α		Ψ^d	
electrode	−/2−[c]	0/−[c]	−/2−[c]	0/−[c]	−/2−[c]	0/−[c]	−/2−[c]	0/−[c]
Pt	−1.864	−1.229	0.016	0.56	0.49	0.70	0.13	0.095
GC	−1.862	−1.228	0.22	1.7	0.61	0.73	0.12	0.093

[a]Mean values of the parameters derived from 15 optimization runs undertaken on the 1st to 7th ac harmonic components. [b]Other experimental and simulation parameters are listed in captions to Figures 6 and S5, Supporting Information. [c]0/− and −/2− relate to the $[Os(\eta^6\text{-pcym})(B_{10}H_{10})]^{0/-}$ and $[Os(\eta^6\text{-pcym})(B_{10}H_{10})]^{-/2-}$ processes, respectively. [d]Calculated using eq 1 for the 1st to 7th ac harmonic components.

DOI: 10.1021/ic503027g
Inorg. Chem. 2015, 54, 4292−4302

obtained with α significantly greater than 0.50 (Table 3). Furthermore, attempts to match the high-frequency experimental ac voltammograms obtained with a Pt electrode for the $[Os(\eta^6\text{-pcym})(B_{10}H_{10})]^{-/2-}$ process and data simulated using the simple model were less successful. These features and the pronounced sensitivity of the kinetics of the $[Os(\eta^6\text{-pcym})(B_{10}H_{10})]^{0/-/2-}$ processes to pretreatment of the electrode surface all support the supposition on mediation of the electron transfer by specific interaction between the osmaborane and the electrode. Thus, FT ac voltammetric studies on $[Os(\eta^6\text{-pcym})(B_{10}H_{10})]$ in acetonitrile (0.10 M $(n\text{-Bu})_4NPF_6$) imply that the reduction processes are probably inner sphere one-electron transfers and, probably, involve specific interaction of the electroactive species with the electrode surface. On this basis, the kinetic parameters shown in Table 3 should be regarded as *apparent* values.

Voltammetry of [1-(η^6-pcym)-1-$OsB_{10}H_{10}$] (8) in $Pyrr_{1,4}$-NTf_2. The formal oxidation state of II for osmium in **8** suggests that $[Os(\eta^6\text{-pcym})(B_{10}H_{10})]$ also should be capable of undergoing oxidation. Dc voltammetry in CH_3CN (0.10 M $(n\text{-Bu})_4NPF_6$) did not reveal oxidation of $[Os(\eta^6\text{-pcym})(B_{10}H_{10})]$ at potentials prior to the background oxidation limit (Figure S2, Supporting Information). Consequently, dc and FT ac cyclic voltammetric analysis of the $[Os(\eta^6\text{-pcym})(B_{10}H_{10})]$ oxidation was further undertaken in the room temperature ionic liquid $Pyrr_{1,4}$-NTf_2, which has a very wide electrochemical window.[59]

As in the molecular solvent acetonitrile, the first $[Os(\eta^6\text{-pcym})(B_{10}H_{10})]^{0/-}$ reduction step was found to be chemically reversible in $Pyrr_{1,4}$-NTf_2 at GC and metal (Pt and Au) electrodes (Figures 7 and S6, Supporting Information). The

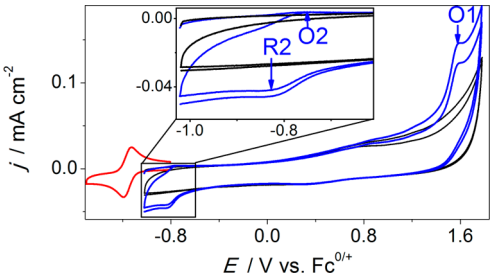

Figure 7. Dc cyclic voltammograms (v = 0.10 V s^{-1}) for reduction (red) and oxidation and reduction (blue) of 1.1 mM $[Os(\eta^6\text{-pcym})(B_{10}H_{10})]$ in $Pyrr_{1,4}$-NTf_2 with a GC electrode at 297 K. Black curves show voltammograms obtained in the absence of $[Os(\eta^6\text{-pcym})(B_{10}H_{10})]$. Inset shows an expanded plot of the outlined region. O1 shows the $[Os(\eta^6\text{-pcym})(B_{10}H_{10})]$ oxidation process, while R2 and O2 show the chemically reversible redox process associated with new electroactive species produced from the oxidized osmaborane cluster.

$E^0_{0/-}$ value of −1.16 V vs $Fc^{0/+}$ derived from voltammetric studies in the ionic liquid via experiment−simulation comparisons was more positive than in CH_3CN by ca. 0.07 V, presumably due to a medium dependence of the standard formal potential of the $Fc^{0/+}$ couple or specific interaction between reduced forms of $[Os(\eta^6\text{-pcym})(B_{10}H_{10})]$ and $Pyrr_{1,4}^+$. A similar difference in E^0 values has been reported for reduction of stilbenes in $Pyrr_{1,4}$-NTf_2 and CH_3CN.[60,61]

The diffusion coefficient of $[Os(\eta^6\text{-pcym})(B_{10}H_{10})]^0$ in $Pyrr_{1,4}$-NTf_2 was estimated to be 1.0×10^{-7} cm^2 s^{-1} by comparison of simulated and experimental dc voltammetric data obtained on the scan rate range of 0.04−0.40 V s^{-1} for the first reduction process. $\alpha_{0/-}$ and $k^0_{0/-}$ in $Pyrr_{1,4}$-NTf_2 with a GC electrode were estimated as 0.50 and 0.010 cm s^{-1}, the latter value being substantially lower than that found in acetonitrile (Table 3). Lower k^0 values in ionic liquids as compared to molecular solvents also have been reported for outer-sphere electron transfer processes such as $Fc^{0/+}$ and attributed to slower solvent reorganization during charge transfer in ionic liquids.[62−65] However, the $[Os(\eta^6\text{-pcym})(B_{10}H_{10})]^{0/-/2-}$ processes are probably not outer-sphere and observed solvent dependence of k^0 may be in reality attributed to the differences in the electrode/electrolyte interfaces in these two media. As in CH_3CN, the second reduction process in $Pyrr_{1,4}$-NTf_2 demonstrated even higher sensitivity to the pretreatment of the electrode and the reproducibility of the voltammetric results was not satisfactory.

Dc cyclic voltammograms obtained for $[Os(\eta^6\text{-pcym})(B_{10}H_{10})]$ in $Pyrr_{1,4}$-NTf_2 with a GC electrode also exhibit an irreversible oxidation process at ca. 1.6 V (O1 in Figure 7). On reversing the potential scan direction, a new reversible couple with E^0 of −0.79 V vs $Fc^{0/+}$ and hence more positive by ca. 0.36 V than that for the $[Os(\eta^6\text{-pcym})(B_{10}H_{10})]^{0/-}$ process emerges in dc voltammograms (Figure 7). Thus, voltammetric oxidation of $[Os(\eta^6\text{-pcym})(B_{10}H_{10})]^0$ is followed by fast transformation into a new type of electroactive species. With a Au electrode, all of these features are obscured by background current in the dc voltammograms (not shown).

FT ac voltammetric studies of the oxidation of $[Os(\eta^6\text{-pcym})(B_{10}H_{10})]$ in $Pyrr_{1,4}$-NTf_2 were undertaken by sweeping the dc potential (vs $Fc^{0/+}$) from an initial value of −0.25 ± 0.08 V to a switching potential of 1.77 ± 0.01 V, then to a negative switching potential of −0.95 ± 0.01 V (blue data in Figures 8 and S7, Supporting Information) or −1.46 ± 0.02 V (red data in Figures 8 and S7, Supporting Information) and, finally, back to the initial potential.

The first to fifth harmonic components with GC and Au electrodes for oxidation of $[Os(\eta^6\text{-pcym})(B_{10}H_{10})]$ are significantly overlapped with the background current. However, in contrast, sixth and higher ac harmonic data generated well-defined faradaic responses associated with the redox transformations of $[Os(\eta^6\text{-pcym})(B_{10}H_{10})]$ that are essentially devoid of background current (Figures 8 and S7, Supporting Information).

As predicted from dc voltammetry, well-defined ac signals for the $[Os(\eta^6\text{-pcym})(B_{10}H_{10})]^{0/+}$ process are detected at ca. 1.6 V in higher-order harmonic components of the FT ac voltammograms (O1 and R1, Figures 8 and S7, Supporting Information). The O1, R1 current ratio is indicative of chemical transformation of $[Os(\eta^6\text{-pcym})(B_{10}H_{10})]^+$ to a new species (as in dc voltammetry), which produces a new process (O2 and R2 in Figure 8 and S6, Supporting Information). O3, R3 signals in Figures 8 and S7, Supporting Information, are associated with the $[Os(\eta^6\text{-pcym})(B_{10}H_{10})]^{0/-}$ process.

On the basis of the dc and FT ac voltammetric observations, reaction Scheme 3 is proposed for electrochemistry of the $[Os(\eta^6\text{-pcym})(B_{10}H_{10})]$ cluster in $Pyrr_{1,4}$-NTf_2. At negative potentials, $[Os(\eta^6\text{-pcym})(B_{10}H_{10})]^0$ can undergo consecutive reversible reductions to yield $[Os(\eta^6\text{-pcym})(B_{10}H_{10})]^-$ and $[Os(\eta^6\text{-pcym})(B_{10}H_{10})]^{2-}$. At positive potentials, $[Os(\eta^6\text{-pcym})(B_{10}H_{10})]^0$ is oxidized to produce short-lived $[Os(\eta^6\text{-pcym})(B_{10}H_{10})]^+$ species, which is irreversibly transformed to an unknown compound $[Os(L)(B_XH_Y)]^+$, perhaps via an internal redox transformation. In principle, polyhedral contraction is a known, but uncommon, process occurring upon

DOI: 10.1021/ic503027g
Inorg. Chem. 2015, 54, 4292−4302

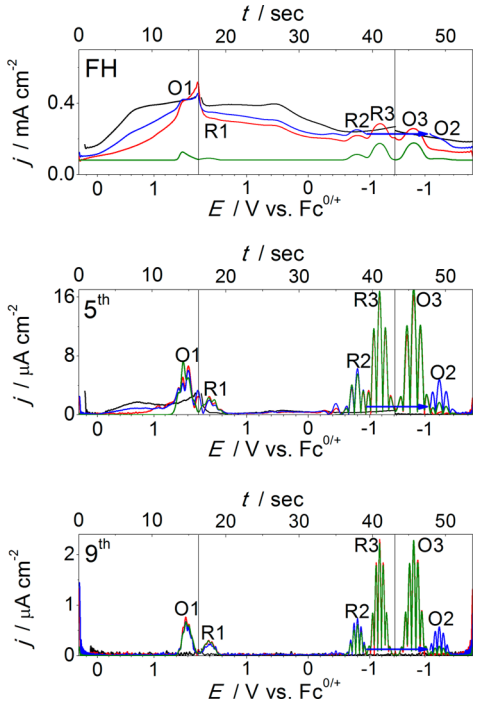

Figure 8. Fundamental, 5th and 9th harmonic components of FT ac voltammograms for oxidation and reduction of 1.1 mM [Os(η^6-pcym)($B_{10}H_{10}$)] in $Pyrr_{1,4}$-NTf_2 with a GC electrode using a negative dc potential limit of ca. −1.0 (blue) and −1.5 V (red), and simulated data (green). Time scale corresponds to red data. Experimental parameters: ν = 0.101−0.121 V s^{-1}; ΔE = 0.16 V; f = 9 Hz. Simulation parameters (see Scheme 3): D = 1.0 × 10^{-7} cm^2 s^{-1} for all species; $E^0_{0/-}$ = −1.160 V, $E^0_{+/0}$ = 1.680 V, $E^0_{X(0/-)}$ = −0.800 V; $k^0_{0/-}$ = 0.010 cm s^{-1}, $k^0_{+/0}$ = 0.016 cm s^{-1}, $k^0_{X(0/-)}$ = 0.0050 cm s^{-1}; α = 0.50 for all processes; k_f^+ = 3.0 × 10^4 s^{-1}, k_b^+ = 1.0 × 10^{-10} s^{-1}; k_f^X = 0.30 s^{-1}, k_b^X = 1.0 × 10^{-10} s^{-1}; R_u = 1900 Ω; C_{dl} = 9.0 μF cm^{-2}.

action of oxidizing agents on metallacarboranes.[66,67] The (R2,O2) process can be associated with an $[Os(L)(B_XH_Y)]^{+/2+}$ reaction. The ac voltammogram simulated with the use of the parameters listed in the caption to Figure 8 satisfactorily matches the experimental data, although whether the kinetic and thermodynamic parameters used in the simulation represent a unique solution cannot be guaranteed.

CONCLUSIONS

A new *closo*-type 11-vertex osmaborane [1-(η^6-pcym)-1-$OsB_{10}H_{10}$] complex has been synthesized and characterized by a range of physical methods, including single-crystal X-ray analysis, which shows that the osmaborane is isostructural with the ruthenium analogue[2,3] and its structure is typical of this class of compounds.

The features of dc and FT ac voltammetry in CH_3CN (0.10 M (n-Bu)$_4$$NPF_6$) and the room temperature ionic liquid $Pyrr_{1,4}$-NTf_2, and EPR spectroscopy after reduction by exhaustive electrolysis in acetonitrile have been used to characterize the redox chemistry. In the molecular solvent acetonitrile, [1-(η^6-pcym)-1-$OsB_{10}H_{10}$] undergoes two well-resolved chemically reversible one-electron reduction processes (E^0 separated by ca. 0.63−0.64 V). The electrode kinetics of the [1-(η^6-pcym)-1-$OsB_{10}H_{10}$]$^{0/-/2-}$ processes, reflected by the k^0 values, are highly sensitive to the nature of the pretreatment and the identity of the electrode surface. At well-polished electrodes, k^0 for the first reduction process is always greater than that for the second and k^0 values obtained at a GC electrode are faster than those found at Pt or Au metal electrodes, as deduced from the analysis of the FT ac voltammetric data. These observations suggest that the electroreduction of [1-(η^6-pcym)-1-$OsB_{10}H_{10}$] is mediated by specific interaction of the compound with the electrode surface.

Well-defined oxidation of [1-(η^6-pcym)-1-$OsB_{10}H_{10}$] at ca. 1.6 V vs $Fc^{0/+}$ was found in the room temperature ionic liquid $Pyrr_{1,4}$ NTf_2, but not in CH_3CN (0.10 M (n-Bu)$_4$$NPF_6$). [1-($\eta^6$-pcym)-1-$OsB_{10}H_{10}$]$^+$, the potential initial oxidation product, is not highly stable and undergoes an irreversible transformation to produce an electrochemically active species.

Analysis of EPR spectra derived from the one-electron reduction of the [1-(η^6-pcym)1-$OsB_{10}H_{10}$] in acetonitrile and analysis of the electron orbital data derived from the DFT calculations suggest that the formal metal center oxidation state in the original unreduced compound **8** is Os^{II}. This observation is consistent with the metal center making a 3o−2e contribution to the cluster-bonding scheme and not 4o−4e, as suggested previously for some isostructural metallaboranes.[2,4,17]

ASSOCIATED CONTENT

Supporting Information

X-ray crystallographic data and CIF file for [Os(η^6-pcym)($B_{10}H_{10}$)]. Figure S1 showing optimized geometries for *closo*-$B_{11}H_{11}^{2-}$, *hypercloso*-$B_{11}H_{11}$, and [Os(η^6-pcym)($B_{10}H_{10}$)].

Scheme 3. Reaction Scheme Proposed for Redox Transformations of [Os(η^6-pcym)($B_{10}H_{10}$)] in $Pyrr_{1,4}$-NTf_2 within the Potential Range Relevant to Figures 7 and 8

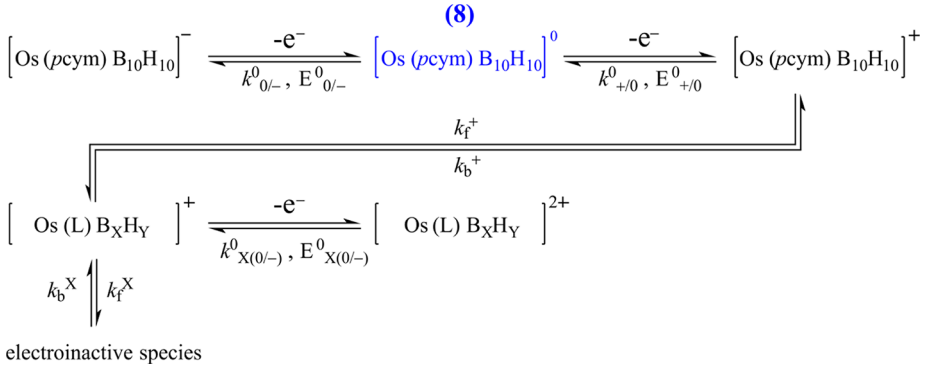

DOI: 10.1021/ic503027g
Inorg. Chem. 2015, 54, 4292−4302

Table S1 listing the Gaussian archive entries for optimized geometries. Table S2 comparing calculated and experimental interatomic distances for $[Os(\eta^6\text{-pcym})(B_{10}H_{10})]$. Table S3 showing molecular orbital coefficients. Figure S2 showing dc cyclic voltammograms for oxidation of $[Os(\eta^6\text{-pcym})(B_{10}H_{10})]$ in CH_3CN. Figure S3 showing dc cyclic voltammetry for reduction and oxidation of $[Os(\eta^6\text{-pcym})(B_{10}H_{10})]^-$ with macrodisk electrodes and near steady-state voltammetry for reduction and/or oxidation of $[Os(\eta^6\text{-pcym})(B_{10}H_{10})]^0$, $[Os(\eta^6\text{-pcym})(B_{10}H_{10})]^-$, and $[Os(\eta^6\text{-pcym})(B_{10}H_{10})]^{2-}$. Table S4 and Figure S4 showing the results of calculation of UV−vis spectra for $[Os(\eta^6\text{-pcym})(B_{10}H_{10})]$, $[Os(\eta^6\text{-pcym})(B_{10}H_{10})]^-$, and $[Os(\eta^6\text{-pcym})(B_{10}H_{10})]^{2-}$. Figure S5 comparing experimental and simulated FT ac voltammograms obtained at a Pt electrode for reduction of $[Os(\eta^6\text{-pcym})(B_{10}H_{10})]$ in CH_3CN (0.10 M $(n\text{-Bu})_4NPF_6$). Figure S6 comparing experimental and simulated FT ac voltammograms for reduction of $[Os(\eta^6\text{-pcym})(B_{10}H_{10})]$ in $Pyrr_{1,4}\text{-}NTf_2$ with a GC electrode. Figure S7 showing FT ac cyclic voltammetry for oxidation and reduction of $[Os(\eta^6\text{-pcym})(B_{10}H_{10})]$ in $Pyrr_{1,4}\text{-}NTf_2$ with a Au electrode. This material is available free of charge via the Internet at http://pubs.acs.org.

AUTHOR INFORMATION

Corresponding Authors

*E-mails: alan.bond@monash.edu.

*E-mails: mark.bown@csiro.au.

Notes

The authors declare no competing financial interest.

ACKNOWLEDGMENTS

The Monash University authors acknowledge financial support from the Australian Research Council.

REFERENCES

(1) Wade, K. *J. Chem. Soc. D* **1971**, 792−793.

(2) Kennedy, J. D. *Inorg. Chem.* **1986**, *25*, 111−112.

(3) Baker, R. T. *Inorg. Chem.* **1986**, *25*, 109−111.

(4) Crook, J. E.; Elrington, M.; Greenwood, N. N.; Kennedy, J. D.; Woollins, J. D. *Polyhedron* **1984**, *3*, 901−904.

(5) Johnston, R. L.; Mingos, D. M. P. *Inorg. Chem.* **1986**, *25*, 3321−3323.

(6) Cotton, F. A.; Wilkinson, G.; Gaus, P. L. *Basic Inorganic Chemistry*, 2nd ed.; John Wiley & Sons, Inc.: New York, 1987; p 296.

(7) Bould, J.; Harrington, R. W.; Clegg, W.; Kennedy, J. D. *J. Organomet. Chem.* **2012**, *721*−*722*, 155−163 and references therein.

(8) King, R. B. *Inorg. Chem.* **1999**, *38*, 5151−5153.

(9) King, R. B. *Inorg. Chim. Acta* **2000**, *300*−*302*, 537−544.

(10) King, R. B.; Hagel, J. *Polyhedron* **2006**, *25*, 3183−3188.

(11) Shameema, O.; Jemmis, E. D. *Inorg. Chem.* **2009**, *48*, 7818−7827.

(12) King, R. B.; Silaghi-Dumitrescu, I.; Sovago, I. *Inorg. Chem.* **2009**, *48*, 10117−10125.

(13) Lupan, A.; King, R. B. *Inorg. Chem.* **2011**, *50*, 9571−9577.

(14) King, R. B.; Silaghi-Dumitrescu, I.; Şovago, I. *Polyhedron* **2012**, *40*, 110−117.

(15) Ghoneim, M. M.; El-Hallag, S. I. *J. Braz. Chem. Soc.* **2010**, *21*, 7−15.

(16) Ghoneim, M. M.; El-Hallag, S. I. *Chin. J. Chem.* **2010**, *28*, 1849−1856.

(17) Bown, M.; Greenwood, N. N.; Kennedy, J. D. *J. Organomet. Chem.* **1986**, *309*, C67−C69.

(18) Bown, M.; Fontaine, X. L. R.; Greenwood, N. N.; Kennedy, J. D. *Z. Anorg. Allg. Chem.* **1991**, *598*−*599*, 45−52.

(19) Bown, M.; Fontaine, X. L. R.; Greenwood, N. N.; Kennedy, J. D.; Thornton-Pett, M. *J. Chem. Soc., Dalton Trans.* **1988**, *1*, 925−930.

(20) Littger, R.; Englich, U.; Ruhlandt-Senge, K.; Spencer, J. T. *Angew. Chem.* **2000**, *39*, 1472−1474.

(21) Bown, M.; Fontaine, X. L. R.; Greenwood, N. N.; Kennedy, J. D. *J. Organomet. Chem.* **1987**, *325*, 233−246.

(22) Hawthorne, M. F.; Pilling, R. L. *Inorg. Synth.* **1967**, *9*, 16−19.

(23) Bown, M.; Fontaine, X. L. R.; Greenwood, N. N.; Kennedy, J. D.; Thornton-Pett, M. *J. Chem. Soc., Dalton Trans.* **1990**, *10*, 3039−3049.

(24) McFarlane, W. *Proc. R. Soc. A* **1968**, *306*, 185−199.

(25) *Apex2*, v2012-2.0; Bruker AXS Inc.: Madison, WI, 2012.

(26) Sheldrick, G. M. *SADABS—Program for Scaling and Empirical Absorption Correction*; University of Göttingen: Göttingen, 1997.

(27) Sheldrick, G. M. *Acta Crsytallogr., Sect. A* **2008**, *64*, 112−122.

(28) Bond, A. M.; Duffy, N. W.; Guo, S.-X.; Zhang, J.; Elton, D. *Anal. Chem.* **2005**, *77*, 186A−195A.

(29) Bard, A. J.; Faulkner, L. R. *Electrochemical Methods: Fundamentals and Applications*, 2nd ed.; John Wiley & Sons, Inc.: New York, 2001.

(30) Janisch, J.; Ruff, A.; Speiser, B.; Wolff, C.; Zigelli, J.; Benthin, S.; Feldmann, V.; Mayer, H. A. *J. Solid State Electrochem.* **2011**, *15*, 2083−2094 and references therein.

(31) Wertz, J. E.; Orton, J. W.; Auzins, P. *Discuss. Faraday Soc.* **1961**, *31*, 140−150.

(32) Hanson, G. R.; Gates, K. E.; Noble, C. J.; Griffin, M.; Benson, S. *J. Inorg. Biochem.* **2004**, *98*, 903−916.

(33) http://www.elchsoft.com/DigiElch/DigiElch7/Default.aspx.

(34) http://www.garethkennedy.net/MECSim.html.

(35) Simonov, A. N.; Morris, G. P.; Mashkina, E. A.; Bethwaite, B.; Gillow, K.; Baker, R. E.; Gavaghan, D. J.; Bond, A. M. *Anal. Chem.* **2014**, *86*, 8408−8417 DOI: 10.1021/ac5019952.

(36) Mashkina, E. A.; Simonov, A. N.; Bond, A. M. *J. Electroanal. Chem.* **2014**, *732*, 86−92.

(37) Frisch, M. J.; Trucks, G. W.; Schlegel, H. B.; Scuseria, G. E.; Robb, M. A.; Cheeseman, J. R.; Scalmani, G.; Barone, V.; Mennucci, B.; Petersson, G. A.; Nakatsuji, H.; Caricato, M.; Li, X.; Hratchian, H. P.; Izmaylov, A. F.; Bloino, J.; Zheng, G.; Sonnenberg, J. L.; Hada, M.; Ehara, M.; Toyota, K.; Fukuda, R.; Hasegawa, J.; Ishida, M.; Nakajima, T.; Honda, Y.; Kitao, O.; Nakai, H.; Vreven, T.; J. Montgomery, J. A., Peralta, J. E.; Ogliaro, F.; Bearpark, M.; Heyd, J. J.; Brothers, E.; Kudin, K. N.; Staroverov, V. N.; Keith, T.; Kobayashi, R.; Normand, J.; Raghavachari, K.; Rendell, A.; Burant, J. C.; Iyengar, S. S.; Tomasi, J.; Cossi, M.; Rega, N.; Millam, J. M.; Klene, M.; Knox, J. E.; Cross, J. B.; Bakken, V.; Adamo, C. C.; Jaramillo, J.; Gomperts, R.; Stratmann, R. E.; Yazyev, O.; Austin, A. J.; Cammi, R.; Pomelli, C.; Ochterski, J. W.; Martin, R. L.; Morokuma, K.; Zakrzewski, V. G.; Voth, G. A.; Salvador, P.; Dannenberg, J. J.; Dapprich, S.; Daniels, A. D.; Farkas, O.; Foresman, J. B.; Ortiz, J. V.; Cioslowski, J.; Fox, D. J. *Gaussian 09, Revision D.01*; Gaussian, Inc.: Wallingford, CT, 2013.

(38) Becke, A. D. *J. Chem. Phys.* **1993**, *98*, 5648−5652.

(39) Crook, J. E.; Elrington, M.; Greenwood, N. N.; Kennedy, J. D.; Thornton-Pett, M.; Woollins, J. D. *J. Chem. Soc., Dalton Trans.* **1985**, *11*, 2407−2415.

(40) Fontaine, X. L. R.; Fowkes, H.; Greenwood, N. N.; Kennedy, J. D.; Thornton-Pett, M. *J. Chem. Soc., Dalton Trans.* **1987**, *10*, 2417−2429.

(41) Kennedy, J. D. In *Multinuclear NMR*; Mason, J., Ed.; Plenum Press: New York, 1987; pp 221−258.

(42) Kennedy, J. D. *Prog. Inorg. Chem.* **1986**, *34*, 211−434.

(43) Johnson, B. G.; Gill, P. M. W.; Pople, J. A. *J. Chem. Phys.* **1993**, *98*, 5612.

(44) Dou, J.; Guo, Q.; Wu, L.; Li, D.; Wang, D.; Wang, H.; Li, Y. *Appl. Organomet. Chem.* **2006**, *20*, 193−202.

(45) Lopez, M. E.; Ellis, D.; Murray, P. R.; Rosair, G. M.; Welch, A. J.; Yellowless, L. J. *Collect. Czech. Chem. Commun.* **2010**, *75*, 853−869.

(46) Scott, G.; McAnaw, A.; McKay, D.; Boyd, A. S. F.; Ellis, D.; Rosair, G. M.; Macgregor, S. A.; Welch, A. J.; Laschi, F.; Rossi, F.; Zanello, P. *Dalton Trans.* **2010**, *39*, 5286−5300.

DOI: 10.1021/ic503027g
Inorg. Chem. 2015, 54, 4292−4302

(47) Kennedy, J. D. *Prog. Inorg. Chem.* **1984**, *32*, 519−680.
(48) Strelets, V. V. *Coord. Chem. Rev.* **1992**, *114*, 1−60.
(49) A paramagnetic Os ion, irrespective of its valence state, must have $S = 1/2$ by virtue of being in the low-spin state. The stable isotopes of Os with nuclear magnetic moments are ^{187}Os (1.64%, $I = 1/2$) and ^{189}Os (16.1%, $I = 3/2$). The other stable isotopes of Os have $I = 0$. The simulation program adds the contributions to the spectrum from $I = 0$ isotopes (a spectrum with axial g values) and the spectra from ^{187}Os and ^{189}Os (both with axial g and A values).
(50) Rieger, P. H. *Coord. Chem. Rev.* **1994**, *135/136*, 203−286.
(51) Dunbar, K. R.; Schelter, E. J.; Tsukerblat, B. S.; Ostrovsky, S. M.; Mirovitsky, V. Yu.; Palii, A. V. *Polyhedron* **2003**, *22*, 2545−2556.
(52) Dunbar, K. R.; Schelter, E. J.; Palii, A. V.; Ostrovsky, S. M.; Mirovitsky, V. Yu.; Hudson, J. M.; Omary, M. A.; Klokishner, S. I.; Tsukerblat, B. S. *J. Phys. Chem. A* **2003**, *107*, 11102−11111.
(53) Neilsen, P.; Toftlund, H.; Bond, A. D.; Boas, J. F.; Pilbrow, J. R.; Hanson, G. R.; Noble, C.; Riley, M. J.; Neville, S. M.; Moubaraki, B.; Murray, K. S. *Inorg. Chem.* **2009**, *48*, 7033−7047.
(54) Vugman, N. V.; Rossi, A. M.; Danon, J. *J. Chem. Phys.* **1978**, *68*, 3152−3157.
(55) Abell, G. C.; Bowman, R. C. *J. Chem. Phys.* **1979**, *70*, 2611−2619.
(56) Takaoka, A.; Gerber, L. C. H.; Peters, J. C. *Angew. Chem., Int. Ed.* **2010**, *49*, 4088−4091.
(57) Royea, W. J.; Hamann, T. W.; Brunschwig, B. S.; Lewis, N. S. *J. Phys. Chem. B* **2006**, *110*, 19433−19442.
(58) McCreery, R. L. *Chem. Rev.* **2008**, *108*, 2646−2687.
(59) O'Mahony, A. M.; Silvester, D. S.; Aldous, L.; Hardacre, D.; Compton, R. G. *J. Chem. Eng. Data* **2008**, *53*, 2884−2891.
(60) Abdul-Rahim, O.; Simonov, A. N.; Rüther, T.; Boas, J. F.; Torriero, A. A. J.; Collins, D. J.; Perlmutter, P.; Bond, A. M. *Anal. Chem.* **2013**, *85*, 6113−6120.
(61) Abdul-Rahim, O.; Simonov, A. N.; Boas, J. F.; Rüther, T.; Collins, D. J.; Perlmutter, P.; Bond, A. M. *J. Phys. Chem. B* **2014**, *118*, 3183−3191.
(62) Tachikawa, N.; Katayama, Y.; Miura, T. *Electrochem. Solid-State Lett.* **2009**, *12*, F39−F41.
(63) Xiao, L.; Dickinson, E. J. F.; Wildgoose, G. G.; Compton, R. G. *Electroanalysis* **2010**, *22*, 269−276.
(64) Kim, D. Y.; Yang, J. C.; Kim, H. W.; Swain, G. M. *Electrochim. Acta* **2013**, *94*, 49−56.
(65) Silvester, D. S.; Compton, R. G. *Z. Phys. Chem.* **2006**, *220*, 1247−1274.
(66) Pisareva, I. V.; Chizhevsky, I. T.; Petrovskii, P. V.; Bregadze, V. I.; Dolgushin, F. M.; Yanovsky, A. I. *Organometallics* **1997**, *16*, 5598−5600.
(67) Jones, C. J.; Francis, J. N.; Hawthorne, M. F. *J. Chem. Soc., Chem. Commun.* **1972**, 900−901; *J. Am. Chem. Soc.* **1972**, *94*, 8391−8399.

DOI: 10.1021/ic503027g
Inorg. Chem. 2015, 54, 4292−4302